IEEE Access
Multidisciplinary | Rapid Review | Open Access Journal

Received 21 June 2022, accepted 29 July 2022, date of publication 4 August 2022, date of current version 10 August 2022.

Digital Object Identifier 10.1109/ACCESS.2022.3196345

RESEARCH ARTICLE

Dual-Band Millimeter-Wave Circularly Polarized Antenna for Mobile Communications

NADA ALAA[1], RANIA A. ELSAYED[1], KHALID F. A. HUSSEIN[2], AND WALID S. EL-DEEB[1]
[1]Electronics and Communications Engineering Department, Faculty of Engineering, Zagazig University, Zagazig 44519, Egypt
[2]Microwave Engineering Department, Electronics Research Institute, Cairo 11843, Egypt

Corresponding author: Khalid F. A. Hussein (fkhalid@eri.sci.eg)

ABSTRACT A novel design of dual-band circularly polarized patch antenna is proposed for millimeter-wave applications of the future generations of mobile communication handsets. The antenna structure is composed of a primary circular patch and four parasitic printed elements. The circular patch has two notches on its perimeter. The primary circular patch is designed to operate at 38 GHz as its first-order resonance with perfect impedance matching over the frequency band (37–38.5 GHz). Four parasitic elements with Y-shaped slots are capacitively coupled to the primary patch to get it operational at an additional higher frequency with perfect impedance matching over a wideband (48.2–50.1 GHz). Defects in the ground plane are made as two square slots. The notches on the circumference of the circular patch and the square slots in the ground plane are aligned to a diagonal that makes 45° with the axis of symmetry of the feeding line. The width of each slot and the diagonal distance between them are the design parameters that can be set to produce circular polarization with satisfactory axial ratio (AR). The outline of the composite planar antenna structure has a square shape so as not to degrade the circular polarization. Also, to satisfy the impedance matching without disturbing the circular polarization, the primary patch is fed through a tapered microstrip line instead of using a microstrip line with inset feed. The achieved gain, AR, and radiation efficiency are 6.6 dBi, 0.6 dB, and 92%, respectively, at 38 GHz and are 6.7 dBi, 1.6 dB, and 75%, respectively, at 50 GHz. The antenna is printed on a substrate of thickness 0.25 mm and the outer dimensions of the planar composite patch structure are 2.9 mm × 2.9 mm. The antenna bandwidth to provide good circular polarization with perfect impedance matching at the same time are 800 MHz (37-37.8 GHz) and 200MHz (49.9-50.1 GHz) for the lower and higher frequency bands, respectively. The proposed antenna is fabricated and its performance assessed by simulation is validated by comparison with the results of microwave measurements. Both the simulation and measurement results show good performance of the proposed antenna over the lower and higher frequency bands of operation.

INDEX TERMS Circular polarization, dual-band, microstrip patch antenna, millimeter-wave, Q-band.

I. INTRODUCTION

The microwave range of the electromagnetic spectrum currently utilized for wireless communications is being crowded due increasing number of users and growing services. Consequently, the lack of resources in mobile communications is going to be an incurable problem in the near future. The unlicensed spectrum of the millimeter wave has a wide bandwidth extending from 30 to 300 GHz and, hence, it can adequately solve the problem and meet the demands of the forthcoming generations of mobile communications. Microstrip patch antennas have the advantages of being light weight, easy fabrication, planar configuration and low cost. To keep the light weight and compact size of portable communication devices, a multi-purpose antenna becomes a preferable choice for wireless communication systems. Multi-band circularly polarized printed antennas of compact size are required for many applications such as mobile handsets, satellites, radars, missiles, aircrafts, remote sensing and biomedical telemetry [1]–[4]. In a wireless communication system, if the transmitter and receiver have linearly polarized antennas, they must have

The associate editor coordinating the review of this manuscript and approving it for publication was Emrecan Demirors.

the same orientation to ensure good reception. This can be a problem in many communication systems like cellular mobile communication systems. To overcome this problem, circularly polarized antennas can be employed because the strength of received signal becomes independent of the orientation of the transmitter and receiver antennas. Circular polarization is widely used to enhance the probability of successful link, weather penetration, performance, spectral efficiency and superior mobility. Circular polarized antennas are important for wireless local area network (WLAN) and radio frequency identification (RFID) [5], [6]. Multi-band antennas can be used for frequency reuse utilization and, hence, they are important for the applications of the 5G and global navigation satellite system (GNSS) [7], [8].

Over the past few years, a lot of research papers have been concerned with multi-band circularly polarized printed antennas. In [1], dual-band operation is achieved by etching two elliptical slots in a wideband linearly polarized patch antenna and in the ground plane to act as band rejection element. Two gaps are etched on the circumference of the two slots to realize circular polarization. The work of [9] proposes a dual-band circularly-polarized cavity-backed slot antenna. In [10], a dual-band circularly polarized antenna is proposed which operates in Ka-band and consists of Archimedean spiral patch fed by 50Ω-feed line through $\lambda/4$ impedance transformer. In [11] a dual-band circularly polarized antenna is designed by introducing four T-shaped slits at the patch edges. The work of [12] proposes a dual-band antenna consisting of a rectangular patch surrounded by a ground in the form of a circular ring. Two printed circles are added to produce circular polarization. This antenna is fed by coplanar waveguide. In [13], dual-band antennas are designed to produce RHCP at the lower band and LHCP at the higher band by using two stacked patches; the upper one is a square patch with asymmetric U-shaped slot whereas the lower one is a square patch. The work of [14] presents a dual-band circularly polarized printed antenna. The antenna design is achieved by truncating the patch from two sides and feeding it by SMA coaxial probe. In [15], two-layer dual-band circularly polarized antenna is proposed. This antenna consists of lower circular patch with cross slot at the patch center and peripheral cuts at boundaries and upper square ring patch with truncated corners. The lower patch is excited by coaxial feed whereas the upper patch is excited by the fringing field of the lower patch. In [16], dual-band linearly and circularly polarized antennas are introduced by embedding meandering slot and four metallic vias. The work of [17] introduces a dual-band circularly polarized antenna where the diagonal corners of the square patch are cut using L-shaped slots that help to achieve RHCP at the lower resonating frequency and LHCP at the higher resonating frequency. The work of [18] proposes a dual band circularly polarized patch antenna fed by a pin soldered in beam forming network layer to be employed for phase only beam shaping with element rotation.

The present work proposes dual-band circularly polarized antenna for operation in the Q-band ($33 - 50$ GHz) that is suitable for many future applications such as mobile communications, satellite applications, radio astronomy, terrestrial microwave communications and automotive radars. The proposed antenna has a planar (printed) structure that is composed of a primary circular patch fed by a tapered microstrip line and four parasitic elements that are capacitively coupled to the primary patch. The planar antenna elements are printed on a high-quality thin dielectric substrate with defected ground structure. This antenna works at 38 and 50 GHz with circular polarization. The antenna resonance at the lower frequency band ($37.7 - 38.3$ GHz) is achieved by setting the primary patch radius to the proper value and the defects in the ground plane help to increase the bandwidth. The antenna operation at the higher frequency band ($48.2 - 50.1$ GHz) is achieved by fine tuning of the dimensions of the four parasitic elements including their separating distances from the primary patch.

The proposed design is aided by simulation using the CST Microwave Studio Suite®. Parametric study of the most important dimensions is performed to arrive at the optimum dimensions of the proposed antenna to achieve impedance matching over the possible widest frequency band and to, simultaneously, achieve circular polarization of the radiated field. The proposed antenna is fabricated and its performance is evaluated by measurement and then compared to the simulation results for verification. The results concerning the performance of the antenna proposed in present work is compared with some previously published work in the last few years.

This paper is organized as follows: Section II describes the proposed patch antenna structure. Section III presents parametric study to arrive at the optimal antenna design. In Section IV, the fabrication process of the proposed antenna is described. The experimental setup for the assessment of the antenna is illustrated in Section V. Section VI presents the results concerned with the performance evaluation of the proposed antenna. Finally, Section VII concludes the important results of this work.

II. STRUCTURE OF THE DUAL-BAND CIRCULARLY POLARIZED ANTENNA

The design of the proposed multiband circularly polarized antenna depends on a circular patch as a primary radiator that is designed to operate with its first-order resonance at 38 GHz. Four secondary (parasitic) elements are capacitively coupled to the primary patch, as shown in Figure 1, for efficient operation at 50 GHz. The resonance at 38 GHz is achieved by setting the dimensions of the circular patch and is not significantly affected by the four parasitic elements. On the other hand, the upper efficient operation at the higher resonant frequency is achieved by controlling the shape and dimensional parameters of the parasitic patch elements to act as a reactive load that eliminates the imaginary part of the antenna input impedance at this frequency.

The primary patch has two notches on its perimeter and the defects of the ground plane are made as two square slots. To produce right-hand circular polarization (RHCP)

the notches of the patch and the square slots of the ground plane are aligned along a diagonal that makes 45° with the axis of symmetry of the feeding microstrip line. The left-hand circular polarization (LHCP) can be achieved by making the notches on the circular patch and the slots in the ground plane aligned to a diagonal that makes −45° (instead of +45°) with the axis of symmetry of the feeding line. The circular polarization is achieved by exciting two degenerate modes with their fields being of equal amplitudes, orthogonal orientations, and 90° phase difference. The symmetry of the patch structure around the 45°-diagonal ensures equal amplitudes and orthogonal orientations of the radiated fields of the two modes. The 90°-phase shift is realized by setting the detailed dimensions of the main patch, parasitic elements, and the defects of the ground plane. This is achieved with the aid of objective parametric study to arrive at the dimensions that gives the best AR. The outline of the composite planar antenna structure has a square shape so as not to degrade the circular polarization. Also, to satisfy the impedance matching without disturbing the circular polarization, the primary patch is fed through a tapered microstrip line instead of using a microstrip line with inset feed.

In the proposed design, it is necessary for circular polarization that the antenna structure has two diagonals about which the antenna geometry is symmetric. The two diagonals should be perpendicular to each other and each of them should make 45° with the axis of the feeding line. In spite of being necessary, this geometrical symmetry is not enough to achieve circular polarization. The structure details and the dimensional parameters should be properly designed to achieve acceptable value of the axial ratio (AR). To achieve the required impedance matching without violating the 45°-diagonal symmetry of the printed antenna structure, it is proposed to use a tapered feed line instead of the commonly used inset-feed. Thus, the dimensional parameters of the printed antenna, presented in Figure 1, should be optimized to simultaneously achieve the design goals over the desired operational frequency bands, i.e., to get $|S_{11}| < -10$ dB and AR < 3 dB. The radius of the circular patch antenna, R_P, determines the frequency at which the first order mode is excited in the cavity below the patch. It can be approximated as follows [20].

$$R_P = F\left\{1 + \frac{2h}{\pi\epsilon_r F}\left[\ln\left(\frac{\pi F}{2h}\right) + 1.7726\right]\right\}^{-1/2},$$
$$F = \frac{8.791\times10^7}{f_0\sqrt{\epsilon_r}} \quad (1)$$

where f_0 is the frequency of the first-order resonance. In the proposed design this frequency is set as $f_0 = 38$ GHz.

The proposed antenna has defecting ground structure (DGS) with the same diagonal of symmetry as the composite patch structure (i.e., the circular patch and the four parasitic elements) to enhance the performance regarding the circular polarization and the impedance matching over the required operational frequency bands. The cavity between the circular patch and the ground plane acts like a semi-closed cavity or open enclosure [19] that is characterized by high Q-factor resonant radiating modes. The cuts made in the ground plane help to increase the bandwidth of cavity resonance and improves the radiation efficiency.

The proposed planar structure is printed on Rogers RO3003 substrate with height, H = 0.25 mm, relative permittivity, $\varepsilon_r = 3$ and dielectric loss tangent, $\tan\delta = 0.001$. The patch and ground plane are made of pure copper with thickness, T = 0.035 mm, and electric conductivity, $\sigma_e = 5.96\times10^7$ S/m. The antenna consists of driving patch and four parasitic patches. The driving patch is circular with radius, R_P, and is directly fed by tapered microstrip feed line to achieve impedance matching. Each of the four parasitic elements looks like a triangle with one of its sides curved to match the circular perimeter of the main patch. Each of the parasitic elements has a Y-shaped cut at its corner. Let the Y-letter be seen as two arms branched from a (vertical) trunk. The Y-slot has a width of W_Y, arm lengths of L_Y, and trunk length of D_Y. The circular polarization is further improved by the cuts in the main patch. The four parasitic elements are capacitively coupled to the main patch and add a reactive load to the antenna impedance that helps to satisfy the resonance (cancellation of the imaginary part at the higher frequency band). The capacitive loading is achieved through edge coupling between the parasitic elements and the main patch.

III. PARAMETRIC STUDY FOR THE OPTIMUM DESIGN OF THE DUAL-BAND ANTENNA

The design methodology followed in the present work depends on an extensive parametric study to arrive at the detailed antenna dimensions that satisfy the best performance including the impedance matching, perfect circular polarization, and high radiation efficiency. In this section, the numerical results obtained by simulation are presented and discussed for the purpose of describing the design process to arrive at the final antenna structure and investigate its performance. The parametric study performed to arrive at the optimal design parameters of the antenna is described in detail, as well. It should be noted that during the process of parametric study, only one dimensional parameter is changed while the other parameters are kept constant.

A. EFFECT OF THE RADIUS OF THE CIRCULAR PATCH

The effect of changing the circular patch radius, R_P, on the magnitude of the reflection coefficient, $|S_{11}|$, at the antenna input port is presented in Figure 2. Changing R_P has the effect of tuning the resonant frequency at the lower frequency band (38 GHz) as shown in Figure 2a. At the higher frequency band (50 GHz) changing R_P has the effect of changing the band width of antenna impedance matching as shown in Figure 2b. More precisely, changing the patch radius, R_P, affects the end frequency of the higher frequency band while keeping the start frequency almost unchanged.

On the other hand, the effect of R_P on the AR is presented in Figure 3. It is shown that this parameter controls the frequency at which the AR is minimum at both the lower and higher frequency bands of antenna operation.

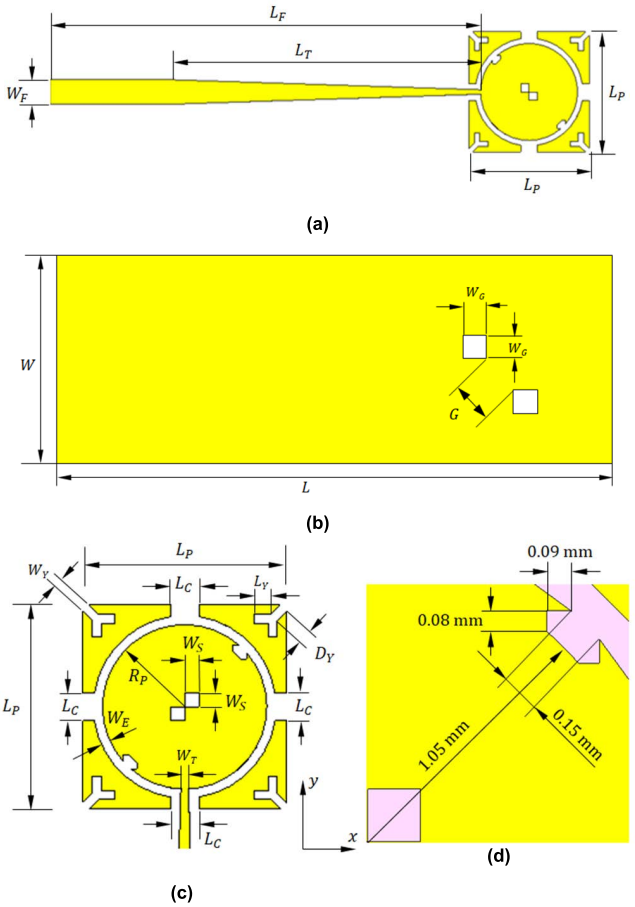

FIGURE 1. Design of the proposed dual-band patch antenna to produce RHCP. (a) Top view of the printed antenna. (b) Bottom view showing the defected ground plane. (c) Details of the patch and parasitic elements (d) Zoomed view in the part of the patch surrounded by red square border.

From this parametric study the value of $R_P = 1.17$ mm is selected to achieve the goals of impedance matching at the desired frequencies (38 and 50 GHz) with excellent impedance matching ($|S_{11}| < -20$ dB) and good circular polarization ($AR < 2$ dB) .

Changing the circular patch radius, R_P, has the effect of changing the frequency response of the maximum gain over the two operational frequency bands of the proposed antenna as presented in Figure 4. It is shown that the gain over the lower frequency band is slightly affected by changing R_P, whereas the gain over the higher frequency band is significantly affected by changing this parameter. Setting $R_P = 1.17$ mm gives a gain of about 6.6 and 6.7 dBi at the frequencies 38 and 50 GHz, respectively.

B. EFFECT OF THE SIDE LENGTH OF THE ANTENNA OUTER BOUNDARY

The dimensional parameter L_P is the side length of the square-shaped outline of the proposed antenna. The effects of changing this parameter, while keeping the parameters R_P, L_C, and W_G constant on the reflection coefficient $|S_{11}|$ and the AR are presented in Figures 5 and 6. As discussed in Section II, the four parasitic elements which are capacitively coupled to the (primary) circular patch control, mainly, the antenna characteristics at the higher frequency band.

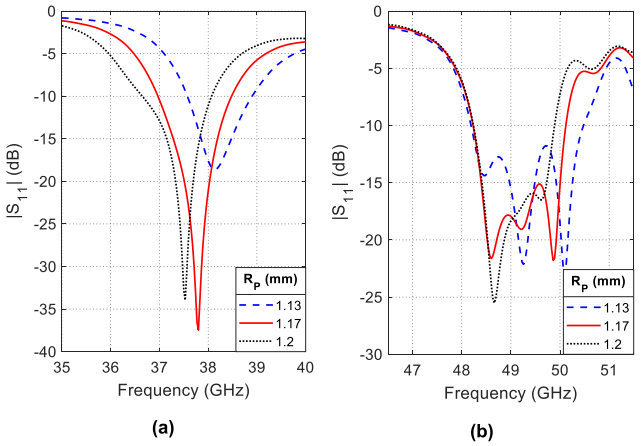

FIGURE 2. Frequency dependence of the reflection coefficient $|S_{11}|$ at the antenna input port for different values of the internal patch radius, R_P.

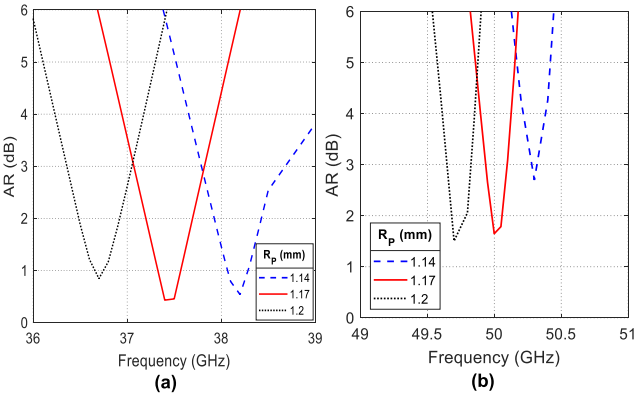

FIGURE 3. Frequency dependence of the AR for different values of the circular patch radius, R_P.

This can be shown in Figure 5 that presents the dependence of $|S_{11}|$ on the frequency for different values of the parameter L_P. Increasing L_P while keeping R_P, L_C, and W_G unchanged means that the area of each parasitic element is increased and, hence, its reactive loading on the primary patch is increased which affects the resonance at 50 GHz. As shown in Figure 5a, changing L_P has almost no effect on $|S_{11}|$ at 38 GHz. On the other hand, changing L_P has major effects on $|S_{11}|$ at the higher frequency band of the antenna. Both the resonant frequency and the band width of this band is strongly dependent on L_P. As regarding the AR, the parameter L_P has major effects at both the lower and higher frequency bands as shown in Figure 6.

The value of $L_P = 2.9$ mm is selected as it results in a low value of $|S_{11}|$ indicating good impedance matching over a wider frequency band than those obtained using $L_P = 2.8$ mm or 3.0 mm. Thus, this parameter is set to $L_P = 2.9$ mm to get the higher frequency band of operation $48.25 - 51.15$ GHz while keeping the same performance at the lower frequency band (38 GHz). Also, the value of $L_P = 2.9$ mm results in $AR < 3dB$ at both the lower and higher frequency bands.

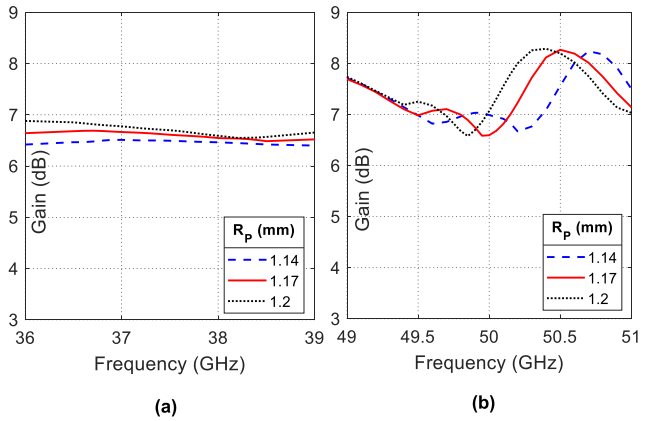

FIGURE 4. Frequency dependence of the max gain for different values of the circular patch radius, R_P.

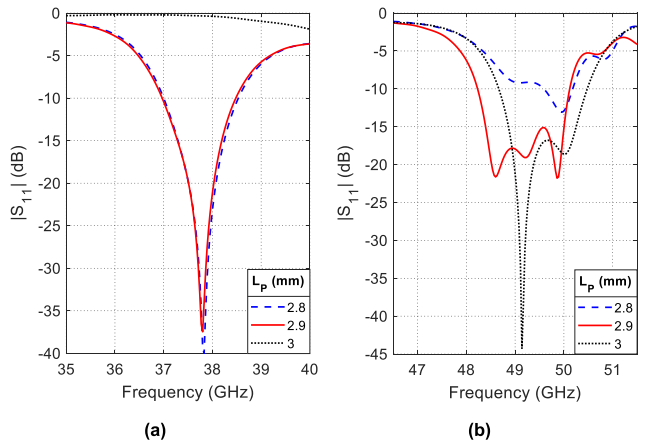

FIGURE 5. Frequency dependence of the reflection coefficient $|S_{11}|$ at the antenna input port for different values of the antenna length, L_P.

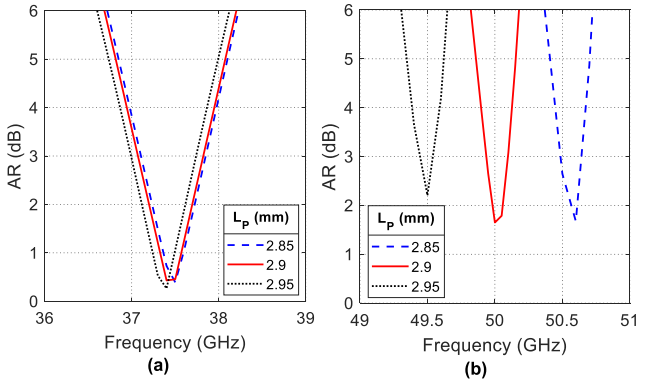

FIGURE 6. Frequency dependence of the AR for different values of the antenna length, L_P.

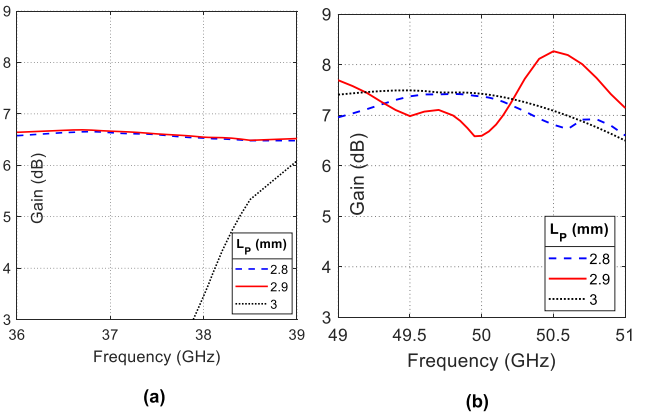

FIGURE 7. Frequency dependence of the max gain for different values of the antenna length, L_P.

Changing the length, L_P, of the antenna outer boundary has the effect of changing the maximum gain over the two operational frequency bands as presented in Figure 7. It is shown that the gain over the two frequency bands is significantly affected by changing this parameter. Setting $L_P = 2.9$ mm gives a gain of about 6.6 and 6.7 dBi at the frequencies 38 and 50 GHz, respectively.

C. EFFECT OF THE SEPARATION BETWEEN THE PARASITIC ELEMENTS

The dimensional parameter L_C is the horizontal and vertical separation distances between the parasitic elements, as shown in Figure 1. The effects of changing L_C on the reflection coefficient $|S_{11}|$ and the AR, respectively over the operational frequency bands are presented in Figures 8 and 9, respectively. It should be noted that, while changing L_C, the other dimensional parameters including W_G (width of the circular gap) are kept constant.

As shown in Figures 8a and 9a, changing L_C has negligible effects on both $|S_{11}|$ and the AR, respectively, over the lower frequency band. On the contrary, the parameter L_C has considerable effects on both $|S_{11}|$ and the AR over the higher frequency band, as shown in Figures 8b and 9b, respectively. This can be attributed to that changing L_C leads to change the size of the parasitic elements which are strongly related to the higher frequency resonance as explained before and have negligible effects on the antenna operation at the lower frequency band. To get the widest frequency band and the minimum AR at 50 GHz, the value of $L_C = 0.4$ mm is selected.

The effect of changing the dimensional parameter L_C, on the maximum gain over the two operational frequency bands are presented in Figure 10. It is shown that the gain over the lower frequency band is almost unaffected by changing L_C, whereas the gain over the higher frequency band is considerably affected by changing this parameter. This can be interpreted as that antenna resonance producing the radiation at the higher frequency band is related to the existence and, hence, the separating distance L_C between the parasitic elements placed around the main patch.

D. EFFECT OF THE Y-SLOT WIDTH OF THE PARASITIC ELEMENTS

The W_Y dimensional parameter is the width of the Y-slot etched on the four parasitic elements. As shown in Figure 11, this parameter has almost no effect on the impedance matching at the lower frequency band (38 GHz), whereas it

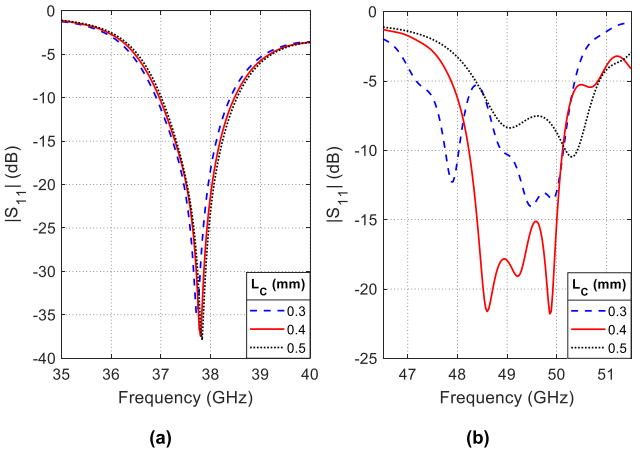

FIGURE 8. Frequency dependence of the reflection coefficient $|S_{11}|$ at the antenna input port for different values of the separation between the parasitic elements, L_C.

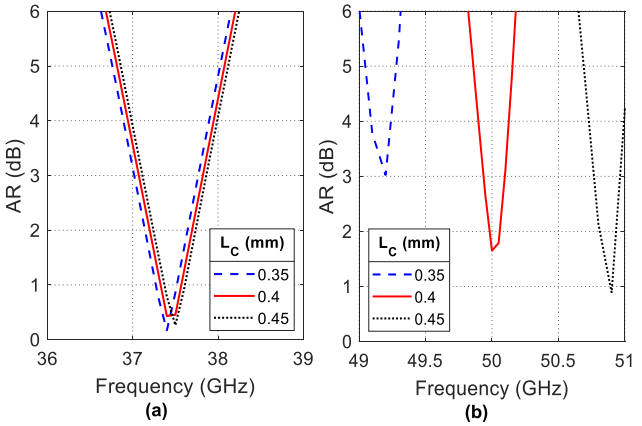

FIGURE 9. Frequency dependence of the AR for different values of the separation between the parasitic elements, L_C.

has major effects on the reflection coefficient $|S_{11}|$ and the bandwidth of the higher frequency band (50 GHz).

As shown in Figure 11, the value of $W_Y = 0.13$ mm gives better impedance matching and wider bandwidth than those obtained for $W_Y = 0.1$ or 0.15 mm. Thus, setting $W_Y = 0.13$ mm enhances the antenna performance over the frequency band 48.25-51.15 GHz while keeping the antenna performance over the lower frequency band at 38 GHz.

On the other hand, setting $W_Y = 0.13$ mm gives the best value of the AR at the higher frequency band without affecting the AR over the lower frequency band, as shown in Figure 12.

The effect of changing the Y-slot width, W_Y, on the maximum gain is presented in Figure 16. It is shown that the gain over the lower frequency band is almost unaffected by changing W_Y, whereas the gain over the higher frequency band is strongly dependent on this parameter. This can be interpreted as that antenna resonance producing the radiation at the higher frequency band is related to the existence and, hence, the dimensions of the parasitic elements placed around the main patch.

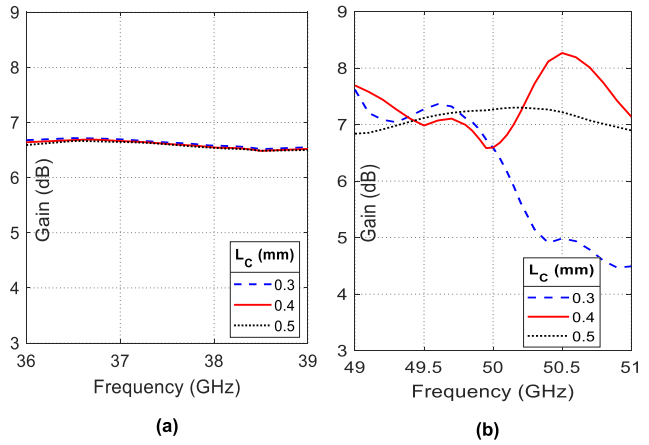

FIGURE 10. Frequency dependence of the max gain for different values of the separation between the parasitic elements, L_C.

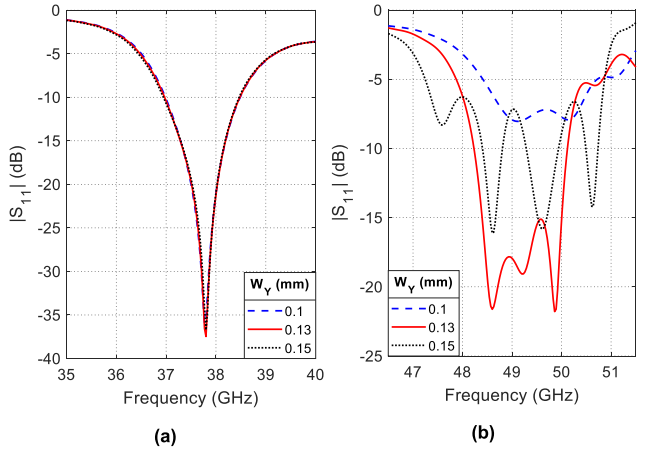

FIGURE 11. Frequency dependence of the reflection coefficient $|S_{11}|$ at the antenna input port for different values of the Y slot width, W_Y.

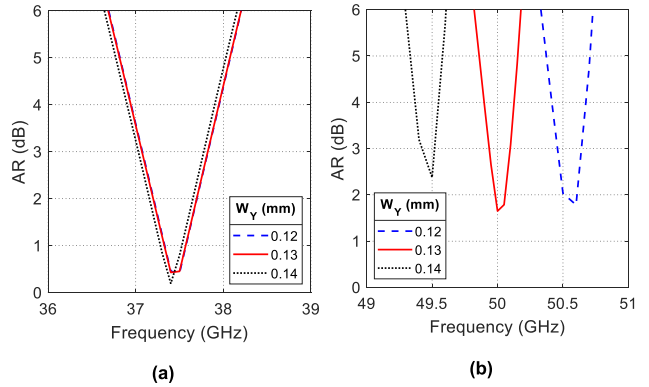

FIGURE 12. Frequency dependence of the AR for different values of the Y slot width, W_Y.

E. EFFECT OF THE SIDE LENGTH OF THE SQUARE CUTS IN THE GROUND PLANE

Changing the width, W_G, of the square cuts made in the ground plane has slight effects on the impedance matching at the lower frequency band of the antenna, as shown in Figure 14a. However, this parameter has major effects on the

magnitude of S_{11} and the impedance matching bandwidth at the higher frequency band, as shown in Figure 14b. On the other hand, the parameter W_G affects the AR at the lower and higher frequency bands of the antenna, as shown in Figure 15a and 15b, respectively.

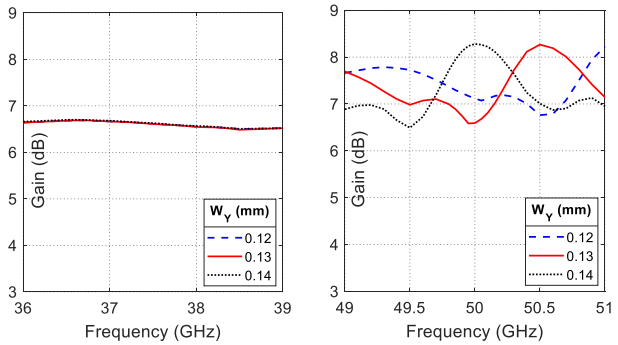

FIGURE 13. Frequency dependence of the max gain for different values of the Y slot width, W_Y.

It is shown that setting $W_G = 0.6\ mm$ gives the best values of the return loss, impedance matching bandwidth and the AR over the two operational bands of the antenna.

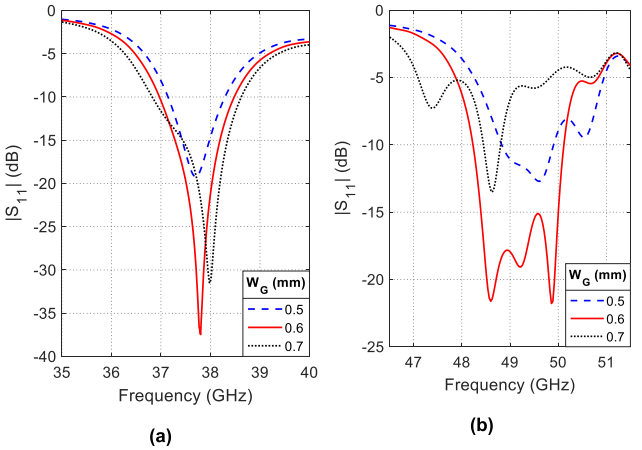

FIGURE 14. Frequency dependence of the reflection coefficient $|S_{11}|$ at the antenna input port for different values of the ground cut width, W_G.

The effect of changing the width, W_G, of the ground cut on the maximum gain are presented in Figure 16. It is shown that the gain over the lower frequency band is slightly affected by changing W_G, whereas the gain over the higher frequency band is strongly dependent on W_G. The value of $W_G = 0.8$ mm gives maximum gain of 6.6 dBi and 6.7 dBi at the lower and higher resonant frequencies, respectively.

F. EFFECT OF THE DISTANCE BETWEEN GROUND CUTS

The diagonal distance, G, between the two square cuts made in the ground plane affects both the impedance matching and the AR at both the lower and higher frequency bands, as shown in Figures 17 and 18. Among the values used to

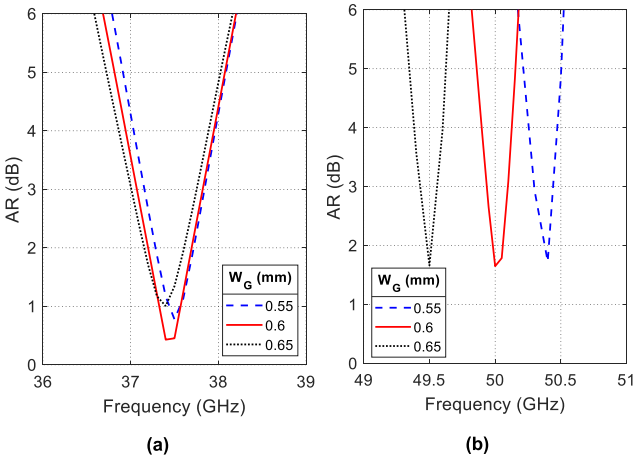

FIGURE 15. Frequency dependence of the AR for different values of the ground cut width, W_G.

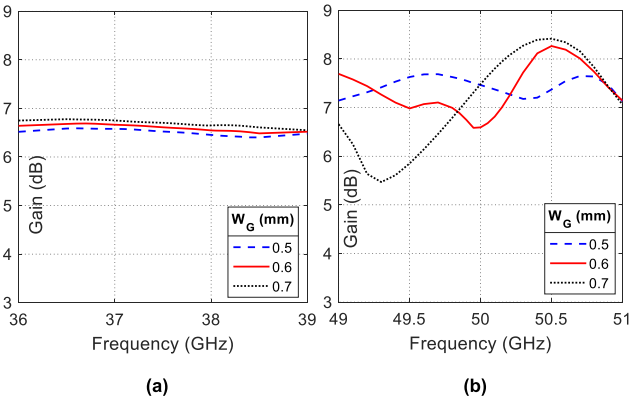

FIGURE 16. Frequency dependence of the max gain for different values of the ground cut width, W_G.

study the effect of this parameter on the antenna performance, it is shown that, the value of $G = 1.41$ mm gives the best impedance matching bandwidth and AR over the two operating bands of the proposed antenna.

Changing the length of the diagonal separation, G, between the ground cuts leads to change the maximum gain over the lower and higher frequency bands as presented in Figure 16. It is shown that the gain over the lower frequency band is almost unaffected by changing G, whereas the gain over the higher frequency band is strongly dependent on G. The value of G = 1.41 mm gives maximum gain of 6.6 dBi and 6.7 dBi at 38 GHz and 50 GHz, respectively.

IV. FINAL DESIGN AND PROTOTYPE FABRICATION

Extensive parametric study has been performed as explained in Section III to arrive at the best values of the dimensional parameters for the antenna design shown in Figure 1. The purpose of the design optimization is to achieve impedance matching ($|S_{11}| < -10\ dB$) and circular polarization ($AR < 3\ dB$) over the lower and upper frequency bands of the antenna operation around 38 and 50 GHz, respectively. The present section summarizes the final values of the design

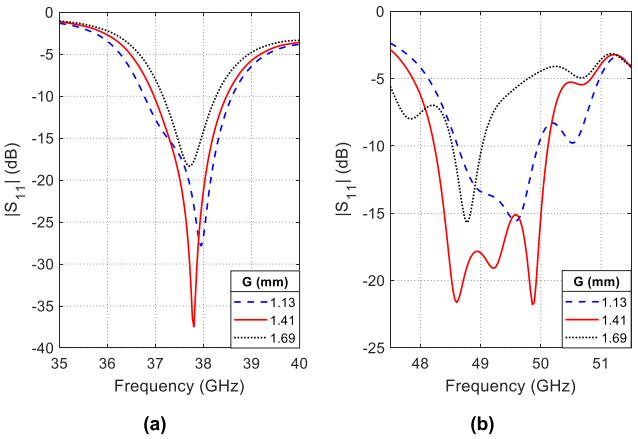

FIGURE 17. Frequency dependence of the reflection coefficient $|S_{11}|$ at the antenna input port for different values of the distance between ground cuts, G.

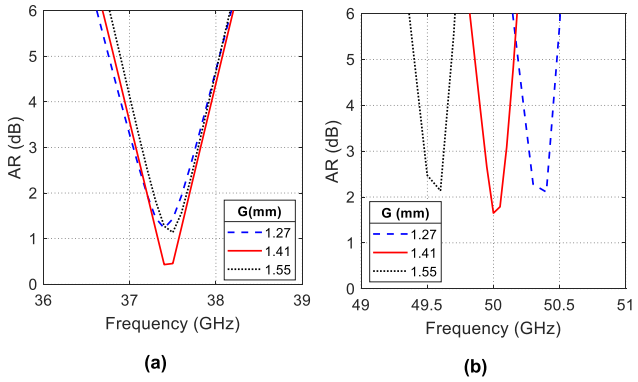

FIGURE 18. Frequency dependence of the AR for different values of the distance between ground cuts, G.

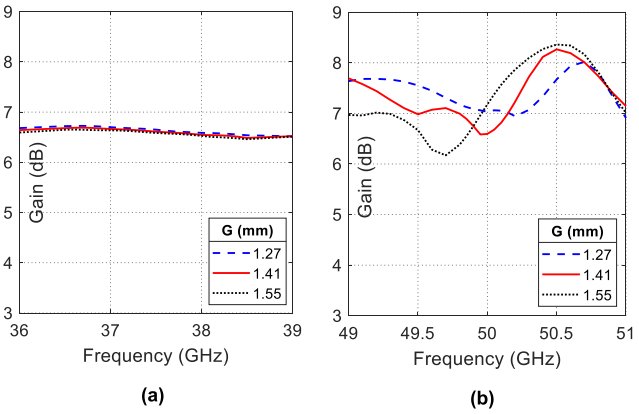

FIGURE 19. Frequency dependence of the max gain for different values of the distance between ground cuts, G.

parameters and describes the process of antenna prototype fabrication according to the final design.

A. FINAL DESIGN PARAMETERS

In this section, the final design of the proposed antenna is given as a list of the final values of the antenna parameters. Based on the parametric study achieved in Section III, the final values of the dimensional parameters of the proposed antenna are listed in Table 1. The antenna is printed on Rogers RO3003 substrate, as described in Section II.

TABLE 1. Values of the dimensional antenna parameters according to the final design.

Dimension	Value (mm)	Description	Dimension	Value (mm)	Description
H	0.25	Substrate height	W_S	0.2	Slot width
T	0.035	Copper thickness	W_F	0.6	Feed line width
W	10	Ground and substrate width	L_F	11.05	Feed line length
L	18.5	Ground and substrate length	L_P	2.9	Parasitic path length
G	1.414	Ground cuts spacing	R_P	1.17	Main patch radius
W_G	0.6	Ground cut width	L_C	0.4	Parasitic patch cut
W_T	0.1	Taper line width at the patch	W_Y	0.13	Y slot width
L_T	7.6	Taper line length	L_Y	0.2	Y arm length
W_E	0.13	Parasitic element gap	D_Y	0.18	Y trunk length

B. PROTOTYPE FABRICATION

In this section, the fabrication process of the antenna prototype is explained. A prototype is fabricated for the antenna proposed in the present work whose design is presented in Figure 1. The dimensional parameters are listed in Table 1. The fabricated prototype is presented in Figure 20. The antenna fabrication is performed using the photolithography technique that can be described in the following procedure.

- Two photo-masks are prepared, one for layout of (top) layer of the composite patch antenna (primary patch, microstrip line, and parasitic elements) and the other for the layout of the (bottom) layer of the defected ground structure. Each mask is made by printing the layout of the corresponding layer on a thin transparent film where the regions corresponding to the metallic (copper) parts are drawn as black (opaque) areas whereas the regions corresponding to bare parts are left transparent.
- A thin substrate of the desired material (Rogers RO3003^{TM} in the present case) and thickness (0.25 mm for the proposed antenna), coated with copper on its top and bottom layers, is covered with photoresist material by means of spin coating.
- The top and bottom layers of the substrate are, then, covered with the corresponding photo-masks for the layouts of the planar antenna and the defected ground. The two masks have been prepared as described in the first step of the fabrication procedure. An alignment mechanism such as an optical camera can be used for aligning the two masks on the top and bottom layers.

- The substrate covered with the photo-masks is then exposed to an intense ultraviolet light to remove the photoresist material coat from regions covered with the transparent areas of the photo-mask (the areas that should be free from copper). The photoresist coat on the remaining regions should be preserved to keep the copper coating.
- The etching process is then carried out as the last stage of the photolithography process. A liquid chemical, like the ferrous chloride, can be used to remove the copper from the top and the bottom faces of the substrate in the areas uncoated by the photoresist material.

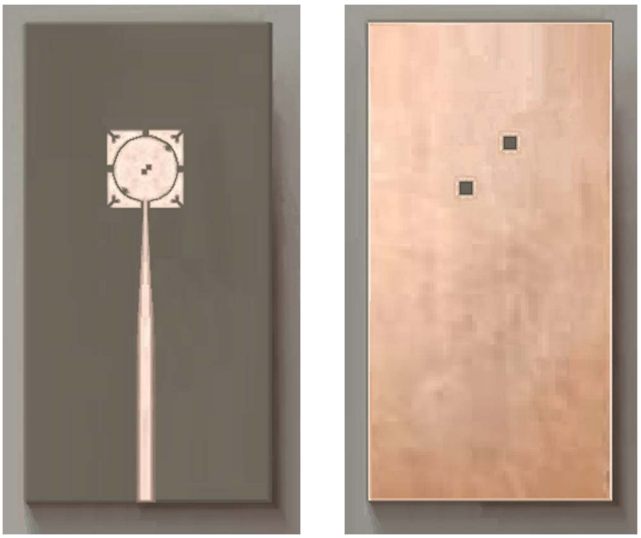

(a) (b)

FIGURE 20. Fabricated prototype of the proposed antenna (a) Front view and (b) Back view.

V. EXPERIMENTAL SETUP FOR PERFORMANCE ASSESSMENT OF THE PROPOSED ANTENNA

The methods of measuring the reflection coefficient at the feeding port of the fabricated antenna and the radiation patterns are explained in detail in the present section. The reflection coefficient and the radiation patterns are measured over the operational frequency bands of the proposed antenna. The equipment, tools, and components used for experimental measurements are listed in Table 2.

TABLE 2. List of the equipment, tools, and components used for experimental measurements.

Device	Model	Frequency Range
Vector Network Analyzer (VNA)	Rhode&Schwartz ZVA67	10 MHz – 67 GHz
Vector Signal Generator (VSG)	Agilent E8267D	100 KHz – 44 GHz
Vector Signal Analyzer (VSA)	Agilent N9010A	10 Hz – 44 GHz
Reference Horn Antenna (20dBi-Gain)	A-Info LB018400	18 – 40 GHz
Reference Horn Antenna (20dBi-Gain)	A-Info LB-12-10-A	40 – 60 GHz

A. EXPERIMENTAL SETUP FOR MEASURING THE REFLECTION COEFFICIENT

The VNA of Rhode and Schwartz model ZVA67 is used for measuring the frequency response of the reflection coefficient, S_{11}, over the frequency bands of interest. An end-launch connector (1.85 mm) and flexible coaxial cable are used for linking the antenna to port 2 of the VNA as shown in Figure 21. The VNA is prepared for measurement by setting the start and stop frequencies, and then performing one-port calibration procedure using the standard mechanical calibration kit model ZV-Z218. For measurement, the fabricated prototype of the proposed antenna is mounted on the coaxial end-launch connector, as shown in Figure 21a. The antenna is then connected to the VNA port 2 through a flexible coaxial cable for the purpose of measuring the reflection coefficient over the frequency band 30-60 GHz, as shown in Figure 21b.

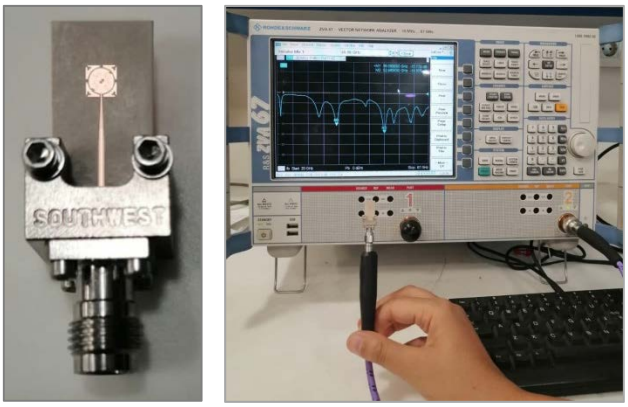

(a) (b)

FIGURE 21. Experimental measurements of the reflection coefficient at the antenna input port (a) Fabricated prototype of the proposed antenna connected to the end launcher. (b) Experimental setup for measurement using the VNA.

B. EXPERIMENTAL SETUP FOR MEASURING THE RADIATION PATTERN

One of the experimental setups that are constructed for measuring the radiation patterns of the proposed antenna is shown in Figure 22. This setup is employed to measure the elevation radiation patterns at 38 GHz using the vector signal generator VSG-E8267D and the vector signal analyzer VSA-N9010A with the A-Info reference-gain horn antennas model LB-018400 (for 18 – 40 GHz band). A similar experimental setup is constructed to measure the radiation patterns at the VNA-ZVA67 with the A-Info reference-gain horn antenna model LB-12-10-A (for 40 – 60 GHz band). The gain and radiation patterns at 50 GHz are measured using the VNA-ZA67 and the reference horn antenna A-Info LB-12-10-A. The experimental setup that employs the VSG and VSA for measuring the gain and radiation patterns of the proposed dual-band circularly-polarized antenna at 38 GHz is presented in Figure 22. The other setup used for measuring the gain and radiation pattern at 50 GHz is similar to the first one except for replacing the VSG and the VSA with the VNA. The received power is assessed by the coefficient of

transmission, $|S_{21}|$, between the antenna under test (placed on a rotator) and the reference-gain linearly-polarized horn antennas.

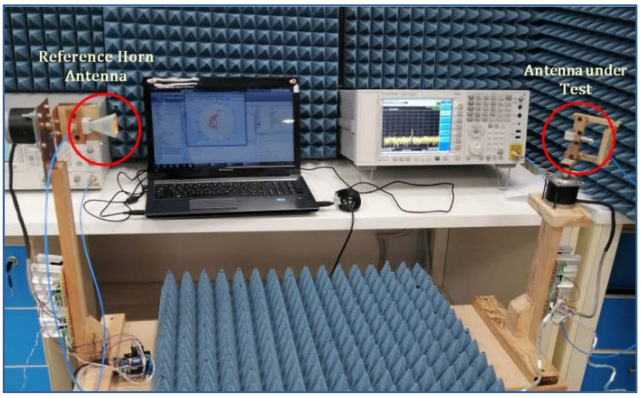

FIGURE 22. Experimental setup for measuring the radiation pattern and gain of the dual-band circularly-polarized antenna using the VSG and VSA.

VI. PERFORMANCE ASSESSMENT OF THE PROPOSED ANTENNA

In this section, the numerical and experimental results are presented and discussed for the purpose of evaluating the performance of the proposed antenna. The antenna performance assessment involves the frequency dependence of the reflection coefficient, S_{11}, at the antenna port, gain, far-field radiation patterns for the total field and the right-hand and left-hand circularly polarized (RHCP, and LHCP, respectively) components and, finally, the axial ratio (AR). The simulation results of the parameter S_{11}, gain, and radiation patterns are compared to the results of experimental measurements for confirmation. The experimental measurements of the reflection coefficient, S_{11}, at the antenna port and the far field radiation patterns are achieved as explained in Section V. The simulation results are compared to the experimental measurements for the purpose of accurate assessment of the antenna performance. The simulation results and experimental measurement are compared to each other for confirmation of the obtained performance parameters. Also, some comparisons with recently published work are presented to demonstrate the proposed antenna performance.

A. FREQUENCY DEPENDENCE OF REFLECTION COEFFICIENT AT THE ANTENNA FEEDING PORT

The frequency dependence of the reflection coefficient, $|S_{11}|$, at the antenna port over a wide range of the frequency ($30-60$ GHz) is obtained by both electromagnetic simulation and experimental measurements. It should be noted that the measurements are carried out using the experimental setup shown in Figure 22. The comparison is presented in Figure 23 showing good agreement between the simulation and experimental results. As shown in this figure, the proposed antenna has two frequency bands; the lower band is centered about 38 GHz whereas, the upper frequency band is centered about 50 GHz. It is shown that, the impedance

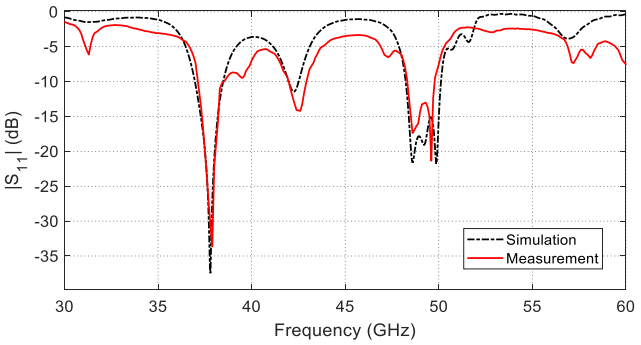

FIGURE 23. Frequency dependence of the reflection coefficient $|S_{11}|$ at the antenna port over a wide range of the frequency obtained by both simulation and experimental measurements.

matching bandwidth ($|S_{11}| < -10$ dB) extends from 36.9 to 38.4 GHz (1.5 GHz, i.e. 3.9%) for the lower frequency band and extends from 48.2 to 50.1 GHz (1.9 GHz, i.e. 3.8%) for the upper frequency band. It is shown that, the experimental measurements agree with the simulation results and both show that antenna impedance is well matched at the operational frequency bands.

Recall that the first resonant frequency 38 GHz is obtained by setting the dimensions of the primary circular patch whereas the second resonance at 50 GHz is obtained by setting the dimensions of the parasitic elements and the width of the coupling gap between them and the primary patch.

B. FAR FIELD PATTERNS OF THE PROPOSED ANTENNA

The radiation patterns of the proposed dual-band circularly-polarized antenna are evaluated by electromagnetic simulation as well as experimental measurement using the setup shown in Figure 22 as described in Section 5.2.

The radiation pattarens of the total field in the elevation planes $\phi = 0°$ and $\phi = 90°$ at 38 GHz are presented in Figure 24 showing that the maximum gain is 6.94 dBi. The radiation pattarens of the total field in the same elevation planes at 50 GHz are presented in Figure 25 showing that the maximum gain is 6.91 dBi. It can be concluded that the radiation pattern is uniform (of circular symmetry) in the azimuthal plane ($\theta = 90°$) with a balloon-like shape in the elevation planes.

C. AXIAL RATIO AND FAR FIELD PATTERNS OF THE CIRCULARLY POLARIZED FIELDS

In this section, the dependence of the AR on the frequency and the radiation patterns of both the co-polarization (RHCP field) and the cross polarization (LHCP field) are presented and discussed. The dependence of the axial ratio on the frequency is presented in Figure 26a and 26b over the frequency ranges around the lower and higher resonant frequencies, respectively. It is shown in Figure 26a, for the lower frequency band the AR is maintained below 3dB over the frequency range $37 - 37.8$ GHz. Thus, the 3dB-AR bandwidth is 800 MHz for the lower frequency band. On the other hand, for the higher frequency band the AR is maintained below 3 dB over the frequency range

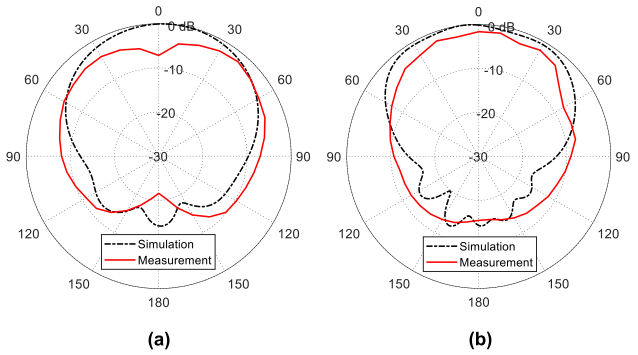

FIGURE 24. Far field patterns of the total field obtained by both simulation and experimental measurements at 38 GHz in the planes (a) $\phi = 0°$ and (b) $\phi = 90°$.

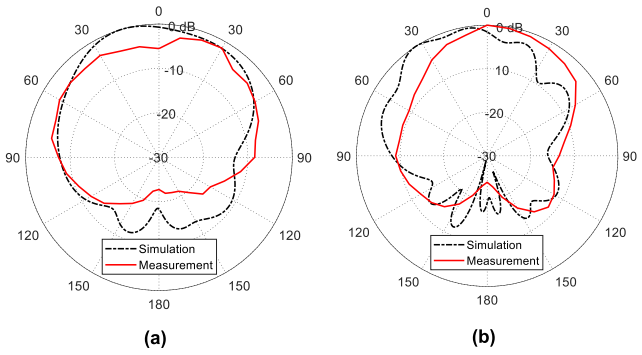

FIGURE 25. Far field patterns of the total radiated field obtained by both simulation and experimental measurements at 50 GHz in the planes (a) $\phi = 0°$ and (b) $\phi = 90°$.

49.9 − 50 GHz. Thus, the 3dB-AR bandwidth is 200 MHz for the higher frequency band of the proposed antenna. The measured values of the AR show good agreement with the results of simulation.

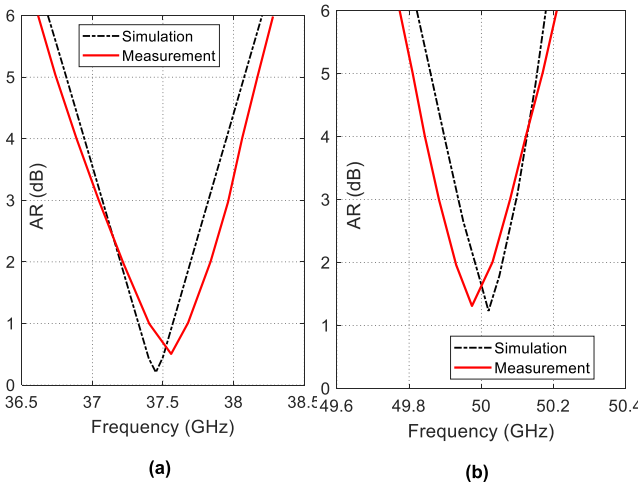

FIGURE 26. Frequency dependence of the AR of the radiated field over a wide range of the frequency.

The radiation patterns of the RHCP and LHCP components of the far field in the elevation planes $\phi = 0°$ and $\phi = 90°$ at 38 and 50 GHz are presented in Figures 27 and 28,

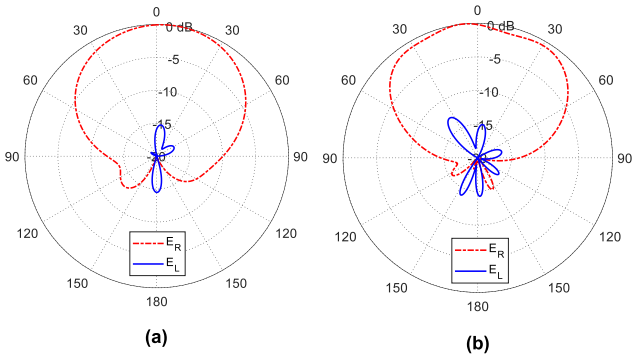

FIGURE 27. Far field patterns of the right-hand and left-hand circularly polarized fields at 38 GHz in the planes (a) $\phi = 0°$ and (b) $\phi = 90°$.

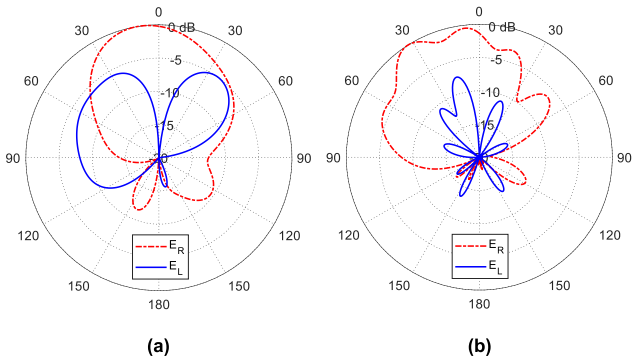

FIGURE 28. Far field patterns of the right-hand and left-hand circularly polarized fields at 50 GHz in the elevation planes (a) $\phi = 0°$ and (b) $\phi = 90°$.

respectively. It is shown that the radiated field in far zone is dominated by RHCP field component. It should be noticed that, the dominance of the RHCP field is attributed to that the line connecting the circumferential notches on the circular patch as well as the line connecting the square apertures of the ground plane make an angle of 45° with the positive x-axis, as shown in Figure 1. To produce LHCP, the antenna design should be modified such that both the line connecting the notches and the line connecting the square apertures of the ground plane make an angle −45° with the positive x-axis.

D. MAXIMUM GAIN AND RADIATION EFFICIENCY OF THE PROPOSED ANTENNA

The frequency dependence of the antenna gain over the two operational frequency bands of the proposed antenna are presented in Figure 29. The average values of antenna gain are about 6.8 and 7.5 dBi over the lower and higher frequency bands, respectively. It is shown that the measured values of the maximum gain come in good agreement with the simulation results.

The radiation efficiency of the proposed antenna over the two operational frequency bands of the proposed antenna are presented in Figure 30. The average values of radiation efficiency are about 90% and 80% over the lower and higher frequency bands, respectively.

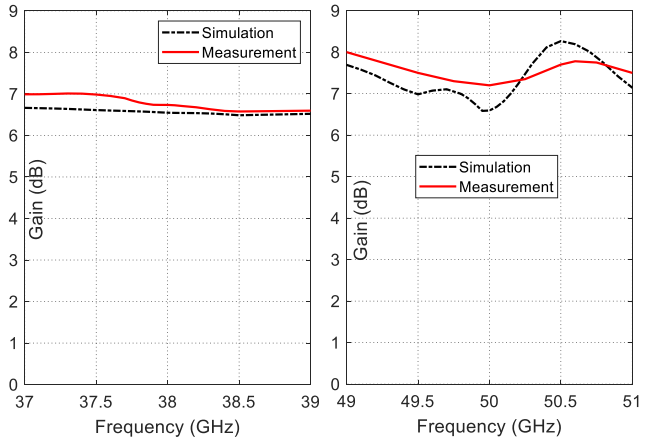

FIGURE 29. Frequency dependence of the maximum gain over a wide frequency range about (a) the first resonant frequency, and (b) the second resonant frequency.

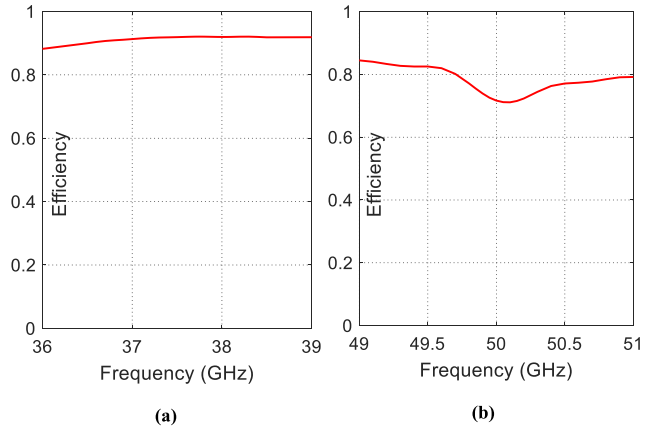

FIGURE 30. Frequency dependence of the radiation efficiency over a wide frequency range about (a) the first resonant frequency, and (b) the second resonant frequency.

TABLE 3. Summary of comparisons with the results of other published work.

Ref.	f_L (GHz)	$\|S_{11}\| < -10$dB BW (GHz)	G (dBi)	AR (dB)	Radiator Size (mm^2)
[9]	37.5	0.4	5	1.1	3.86 × 3.86
	47.8	0.65	5.7	1.19	
[10]	29	1.3	6.66	2.65	4.6 × 4.6
	38	2.4	5.06	2.6	
[21]	28	0.4	7.71	20.86	3.05 × 3.02
	38	0.8	7.9	11.4	
[22]	28	0.9	7.5	1.8	3 × 3
	38	1.3	7.7	0.33	
[23]	27.9	0.85	4	1.5	3.1 ×3.1
	38.1	0.75	4.5	1.7	
Present work	37.8	1.5	6.94	2.84	2.9 × 2.9
	50	1.9	6.91	1.69	

E. SUMMARY OF ANTENNA PERFORMANCE AND COMPARISON WITH PUBLISHED WORK

Some comparative performance measures are listed in Table 3 for comparing the performance of the proposed antenna to some of those presented in recent publications concerned with printed mm-wave antennas designed for the forthcoming generations of mobile communications. From such comparisons, it is shown that the comparison indicates that, the proposed antenna has a relatively small size with good performance over the two operational frequency bands.

VII. CONCLUSION

The present work introduces a dual-band circularly polarized patch antenna for millimeter-wave communications. The antenna is printed on a Rogers' RO3003 substrate of thickness 0.25 mm and the outer dimensions of the planar composite patch structure are 2.9 mm × 2.9 mm. The antenna operates over the lower frequency band (37 – 38.5 GHz) and the higher frequency band (48.2 – 50.1 GHz). The antenna is composed of a primary circular patch and four parasitic printed elements and printed on a thin substrate with DGS. The circular patch has two notches on its perimeter. The defects of the ground plane are made as two square slots. The notches on the circumference of the circular patch and the square slots in the ground plane are aligned on a diagonal that makes 45° with the axis of symmetry of the feeding line. Each of the four parasitic elements is a triangle with arc-shaped base and right-angle corner and has Y-shaped slot at the corner. The achieved gain, AR, and radiation efficiency are 6.6 dBi, 0.6 dB, and 92%, respectively, at 38 GHz and are 6.7 dBi, 1.6 dB, and 75%, respectively, at 50 GHz. The antenna bandwidth to provide good circular polarization with perfect impedance matching at the same time are 800 MHz (37-37.8 GHz) and 200MHz (49.9-50.1 GHz) for the lower and higher frequency bands, respectively. The antenna performance is evaluated by simulation and is validated by comparison with the results of microwave measurement. Both the simulation and measurement results show good performance over both the lower and higher frequency bands of operation.

REFERENCES

[1] Gunaram, J. K. Deegwal, and V. Sharma, "Dual band circular polarized printed dipole antenna for S and C band wireless applications," *Prog. Electromagn. Res. C*, vol. 105, pp. 129–146, 2020.

[2] H. Nawaz, A. U. Niazi, and M. Ahmad, "Dual circularly polarized patch antenna with improved interport isolation for S-band satellite communication," *Int. J. Antennas Propag.*, vol. 2021, Sep. 2021, Art. no. 8022207, doi: 10.1155/2021/8022207.

[3] K. Saraswat and A. R. Harish, "A dual band circularly polarized 45° rotated rectangular slot antenna with parasitic patch," *AEU, Int. J. Electron. Commun.*, vol. 123, Aug. 2020, Art. no. 153260, doi: 10.1016/j.aeue.2020.153260.

[4] K. Goodwilll, N. Singh, and M. V. Kartikeyan, "Dual band circular polarized bow tie slotted patch antenna over high impedance surface for WiMAX application," *Int. J. Microw. Wireless Technol.*, vol. 12, no. 4, pp. 303–308, May 2020, doi: 10.1017/S1759078719001326.

[5] X. Yang, Y. Zhao, J. Pan, K. Sun, and D. Yang, "A circularly polarized microstrip patch antenna with enhanced bandwidth based on substrate integrated waveguide techniques," *Int. J. RF Microw. Comput.-Aided Eng.*, vol. 31, no. 7, Jul. 2021, Art. no. e22669, doi: 10.1002/mmce.22669.

[6] G. G. V. Nitin and D. Kandimalla, "2.4 GHz circularly polarized microstrip patch antenna with diagonal structural symmetry," in *Proc. IEEE Indian Conf. Antennas Propogation (InCAP)*, Dec. 2018, pp. 1–4, doi: 10.1109/INCAP.2018.8770818.

[7] C. Li, X.-Q. Wu, and S. Wang, "A H-shaped dual-band microstrip patch antenna with large frequency ratio under dual modes," in *Proc. IEEE Asia–Pacific Microw. Conf. (APMC)*, Dec. 2020, pp. 822–824, doi: 10.1109/APMC47863.2020.9331593.

[8] E. S. Misbah Un Noor and M. I. Khattak, "Design and analysis of dual-band microstrip patch antenna array for 5G cellular communication networks with improved radiation characteristics," in *Proc. 2nd Int. Conf. Latest Trends Electr. Eng. Comput. Technol. (INTELLECT)*, Nov. 2019, pp. 1–6, doi: 10.1109/INTELLECT47034.2019.8954981.

[9] Q. Wu, J. Yin, C. Yu, H. Wang, and W. Hong, "Low-profile millimeter-wave SIW cavity-backed dual-band circularly polarized antenna," *IEEE Trans. Antennas Propag.*, vol. 65, no. 12, pp. 7310–7315, Dec. 2017, doi: 10.1109/TAP.2017.2758165.

[10] H. Chen, Z. Zhang, and F. Lei, "A design of dual-band circularly polarized millimeter-wave microstrip antenna," in *Proc. IEEE Int. Symp. Antennas Propag. USNC/URSI Nat. Radio Sci. Meeting*, Jul. 2018, pp. 1827–1828, doi: 10.1109/APUSNCURSINRSM.2018.8609398.

[11] K.-P. Yang and K.-L. Wong, "Dual-band circularly-polarized square microstrip antenna," *IEEE Trans. Antennas Propag.*, vol. 49, no. 3, pp. 377–382, Mar. 2001.

[12] O. H. Hassan, S. I. Shams, and A. M. M. A. Allam, "Dual-band circularly polarized antenna with CPW feeding structure," in *Proc. Asia–Pacific Microw. Conf.*, Dec. 2010, pp. 2052–2055.

[13] P. Nayeri, K.-F. Lee, A. Z. Elsherbeni, and F. Yang, "Dual-band circularly polarized antennas using stacked patches with asymmetric U-slots," *IEEE Antennas Wireless Propag. Lett.*, vol. 10, pp. 492–495, 2011, doi: 10.1109/LAWP.2011.2153820.

[14] N. Zakaria, S. K. A. Rahim, T. S. Ooi, K. G. Tan, A. W. Reza, and M. S. A. Rani, "Design of stacked microstrip dual-band circular polarized antenna," *Radioengineering*, vol. 21, pp. 1–6, Sep. 2012.

[15] S. Kumar, B. K. Kanaujia, M. K. Khandelwal, and A. K. Gautam, "Stacked dual-band circularly polarized microstrip antenna with small frequency ratio," *Microw. Opt. Technol. Lett.*, vol. 56, no. 8, pp. 1933–1937, Aug. 2014, doi: 10.1002/mop.28482.

[16] J. Zhang, X. Lin, J. Yu, and L. Nie, "Dual-band linearly and circularly polarized microstrip patch antennas with meandering slot and metallic vias," *Int. J. Microw. Wireless Technol.*, vol. 9, no. 2, pp. 341–348, Mar. 2017, doi: 10.1017/S1759078715001403.

[17] M. P. Joshi and V. J. Gond, "Circularly polarized dual frequency square microstrip patch antenna," in *Proc. IEEE Indian Conf. Antennas Propag. (InCAP)*, Dec. 2018, pp. 1–4, doi: 10.1109/INCAP.2018.8770917.

[18] E. Pelliccia, R. V. Gatti, P. Angeletti, and G. Toso, "A dual-band circularly polarized patch array antenna for phase-only beam shaping with element rotation," *Electronics*, vol. 10, no. 6, p. 643, Mar. 2021, doi: 10.3390/electronics10060643.

[19] K. F. A. Hussein, "Effect of internal resonance on the radar cross section and shield effectiveness of open spherical enclosures," *Prog. Electromagn. Res.*, vol. 70, pp. 225–246, 2007, doi: 10.2528/PIER07012101.

[20] Z. Hasan, A. Zaman, and A. Ahmed, "Design and fabrication of a circular microstrip patch antenna for GPS application," *Int. J. Electron. Commun. Technol.*, vol. 8, no. 3, pp. 54–57, Jul./Sep. 2017.

[21] J. Khan, D. A. Sehrai, and U. Ali, "Design of dual band 5G antenna array with SAR analysis for future mobile handsets," *J. Electr. Eng. Technol.*, vol. 14, no. 2, pp. 809–816, Mar. 2019, doi: 10.1007/s42835-018-00059-9.

[22] S. S. Singhwal, B. K. Kanaujia, A. Singh, and J. Kishor, "Dual band circularly polarized antenna for Ka band applications," in *Proc. Women Inst. Technol. Conf. Electr. Comput. Eng. (WITCON ECE)*, Nov. 2019, pp. 159–161, doi: 10.1109/WITCONECE48374.2019.9092904.

[23] H. Aliakbari, A. Abdipour, R. Mirzavand, A. Costanzo, and P. Mousavi, "A single feed dual-band circularly polarized millimeter-wave antenna for 5G communication," in *Proc. 10th Eur. Conf. Antennas Propag. (EuCAP)*, Apr. 2016, pp. 1–5, doi: 10.1109/EuCAP.2016.7481318.

NADA ALAA received the B.Sc. degree in engineering and the M.Sc. degree in electronics and communications engineering from Zagazig University, Egypt, in 2018. She was a Demonstrator at the Department of Electronics and Communications, Zagazig University, where she is currently a Teaching Assistant with the Department of Electronics and Communications Engineering, Faculty of Engineering. She has published articles in her research areas. Her research interests include antenna and microwave engineering.

RANIA A. ELSAYED received the M.Sc. degree in electronics and communications engineering and the Ph.D. degree in electrical and computer engineering from Zagazig University, Egypt, in 2009 and 2018, respectively. She is currently a Doctor with the Department of Electronics and Communications Engineering, Faculty of Engineering, Zagazig University.

KHALID F. A. HUSSEIN received the B.Sc., M.Sc., and Ph.D. degrees from the Department of Electronics and Electrical Communications, Faculty of Engineering, Cairo University, 1990, 1995, and 2001, respectively. He is currently a Professor with the Department of Microwave Engineering, Electronics Research Institute. He has work experience in scientific research for more than 29 years. He has teaching experience in engineering colleges in many universities for more than 20 years. He has supervised more than 70 doctoral and master's theses. He has published more than 100 papers in international, regional, and local scientific journals and conferences. He was the Head of the Microwave Engineering Department at the Electronics Research Institute for up to four years. He has been a member of the Egyptian Space Program (currently the Egyptian Space Agency) for more than eight years. He has worked as the Principal Investigator for four research projects and the Head of Research Group in four other research projects. He designed and implemented several satellite antennas between prototypes and finished products. He has provided scientific consultations and conducted field measurements related to the design and distribution of mobile communication base station antennas for good signal coverage in behalf of many Egyptian and international companies. His research interests include antennas, electromagnetic wave propagation, risk assessment of human exposure to microwave radiation, optical communications, photonics, quantum computing, radar systems, particularly ground penetrating radar (GPR), synthetic aperture radar (SAR), and remote sensing systems.

WALID S. EL-DEEB received the M.Sc. degree in electronics and communications engineering from Zagazig University, Egypt, in 2004, and the Ph.D. degree in electrical and computer engineering from the University of Calgary, Canada, in March 2011. He joined as a Research and Teaching Assistant at the iRadio Laboratory, University of Calgary, in January 2007, where he was a Postdoctoral Fellow, till August 2011. He is currently an Associate Professor with the Department of Electronics and Communications Engineering, Faculty of Engineering, Zagazig University. He has published many research articles in his research fields in IEEE and other highly ranked journals. His research interests include RF, antenna, and microwave engineering.